

Ring shaped 6.7 GHz methanol maser emission around a young high-mass star

A. Bartkiewicz¹, M. Szymczak¹, and H.J. van Langevelde^{2,3}

¹ Toruń Centre for Astronomy, Nicolaus Copernicus University, Gagarina 11, 87-100 Toruń, Poland

² Joint Institute for VLBI in Europe, Postbus 2, 7990 AA Dwingeloo, The Netherlands

³ Sterrewacht Leiden, Postbus 9513, 2300 RA Leiden, The Netherlands

Received 03 August 2005 / Accepted 14 September 2005

Abstract. We report on EVN imaging of the 6.7 GHz methanol maser emission from the candidate high-mass protostar G23.657-0.127. The masers originate in a nearly circular ring of 127 mas radius and 12 mas width. The ring structure points at a central exciting object which characteristics are typical for a young massive star; its bolometric luminosity is estimated to be $\leq 3.2 \times 10^4 L_{\odot}$ and $\leq 1.2 \times 10^5 L_{\odot}$ for near (5.1 kpc) and far (10.5 kpc) kinematic distances, respectively. However, the spatial geometry of the underlying maser region remains ambiguous. We consider scenarios in which the methanol masers originate in a spherical bubble or in a rotating disc seen nearly face-on.

Key words. masers – stars: formation – stars: circumstellar matter – ISM: individual: (G23.657–0.127)

1. Introduction

Methanol maser emission at 6.7 GHz is a well established tracer of high-mass star-forming regions (Menten 1991). When studied on milliarcsecond (mas) scales (a few hundreds of AU at the distances of a few kpc) it shows various morphologies (Norris et al. 1998; Phillips et al. 1998; Walsh et al. 1998; Minier et al. 2000; Dodson et al. 2004). It has been argued that arc-like or curved structures can be produced by inclined discs (Norris et al. 1998), while linear structures originate in a fraction of the discs which are seen exactly edge-on, resulting in strong masers through radial amplification (Minier et al. 2000).

The hypothesis that 6.7 GHz masers originate in circumstellar discs has difficulty explaining approximately 60% of the methanol masers, which do not show a linear or curved morphology (Phillips et al. 1998; Walsh et al. 1998). It appears that for most of those sources the maser morphology can be explained by a shock wave model (Walsh et al. 1998). Dodson et al. (2004) suggested a model where methanol masers form in planar shocks, and their velocity gradients arise from the rotation of the underlying molecular cloud. Although not in all cases a (detectable) HII region need to have formed, such models are backed up by occasional close associations with nearby (ultra-) compact HII regions. Elitzur (1992) argued that methanol masers arise in a layer of cool dense dust and gas between the shock and ionization fronts around compact HII regions. However, the lack of any observation of the expected symmetric distribution of methanol emission was one argument against this hypothesis.

In this letter we report on the discovery of a well-defined ring structure in the 6.7 GHz methanol maser line, coincident with the IR detection of a young embedded star. This distribution readily offers constraints on the origin of methanol masers by directly determining the separation of the excited region and the young star. The striking geometry warrants a discussion of the underlying three-dimensional structure of methanol masers. We show that the current observations can still be interpreted in more than one model, but future observations will allow us to disentangle this geometry.

2. Observations and data reduction

The source G23.657–0.127 was detected in the unbiased Toruń survey (Szymczak et al. 2002) and displayed a rather complex and relatively faint spectrum. Its position was determined subsequently with a $0''.1$ accuracy by MERLIN single-baseline observations. Then the methanol transition at 6668.519 MHz was observed on 2004 November 11 with eight antennas (Cambridge, Darnhall, Effelsberg, Medicina, Noto, Onsala, Toruń and Westerbork) of the European VLBI Network (EVN)¹ as part of a larger sample. The total on-source time was about 41 min at different hour angles. The phase-referencing scheme used J1825–0737 (240 mJy at 6.7 GHz), separated by $2''.4$ from the target. The bandwidth was 2 MHz in both circular hands, covering LSR velocities from 52 to 141 km s^{−1},

¹ The European VLBI Network is a joint facility of European, Chinese, South African and other astronomy institutes funded by their national research councils.

divided into 1024 channels yielding a velocity resolution of 0.09 km s^{-1} .

The data calibration and reduction were carried out with standard procedures for spectral line observations using the Astronomical Image Processing System (AIPS). The phase referencing yields absolute position of the target and the accuracy is estimated to be 12 mas in Dec and 10 mas in RA. For detailed analysis the target was then self-calibrated on a strong (3.6 Jy) and point-like maser spot identified at 82.6 km s^{-1} . An area of $1 \times 1 \text{ arcsec}^2$ was searched for emission over the entire band. The analysis was carried out on images obtained with natural weighting and a resulting beam of $5.5 \text{ mas} \times 16 \text{ mas}$ at a position angle of -1° . The resulting rms noise level (1σ) in line-free channels was $3.7 \text{ mJy beam}^{-1}$. These observations are among the first EVN 5 cm results with 8 antennas, and the superior image quality allows the detection of many weak features. The calibration and data reduction procedures will be described in more detail in a forthcoming paper.

3. Results

Methanol maser emission was detected over a range of 10.8 km s^{-1} between 77.0 to 87.8 km s^{-1} (Fig. 1). This velocity range is similar to that reported for other sources (Szymczak et al. 2005). The central velocity of the methanol maser profile is 82.4 km s^{-1} . An image integrated over all spectral channels containing emission (Fig. 1) shows that the masers are distributed in a ring. We registered 315 maser spots brighter than 10σ in individual channel maps, which were found to be clustered into 31 maser components. Their brightness temperatures range from 2×10^7 to 10^9 K . The masers appear to be absent from the western portion of the ring and only weak emission is seen in the north-west. We note that about 31% of the flux is missing in the VLBI data, as compared to the single dish observation (Fig.1). Taking into account a 10% accuracy of the flux calibration of both observations, there is a significant excess of the single dish emission over the velocity range 80.6 to 82.2 km s^{-1} , resolved out by the VLBI observations.

Rigorous analysis of the data shows that the distribution of maser components can be fitted by an ellipse with major and minor semi-axes of 133 and 123 mas, respectively. The major axis is elongated along the position angle of $-9^\circ.6$ (Fig. 1). The position of the centre (Table 1) was determined by minimizing the distance between all the maser spots (flux-weighted) and the model ellipse.

Since the maser morphology differs by less than 8% from a circular ring we used the AIPS task IRING to determine the radial distribution of the maser emission (Fig. 2). The mean radius is 127 mas and the width that contains 50% of the flux is 12 mas. The inner and outer radii measured at 10% and 90% of the cumulative flux are 116 and 145 mas, respectively. We conclude that the methanol masers originate in a thin shell with a width of 29 mas ($\sim 20\%$ of the radius), which has a sharp inner edge and a more shallow outer border.

Looking at the detailed velocity structure of the masers, we found that 15 out of 31 maser components display clear spatially coherent filaments or arcs. They have sizes from 4 mas to 29 mas with internal velocity gradients from $16 \text{ m s}^{-1} \text{ mas}^{-1}$ to

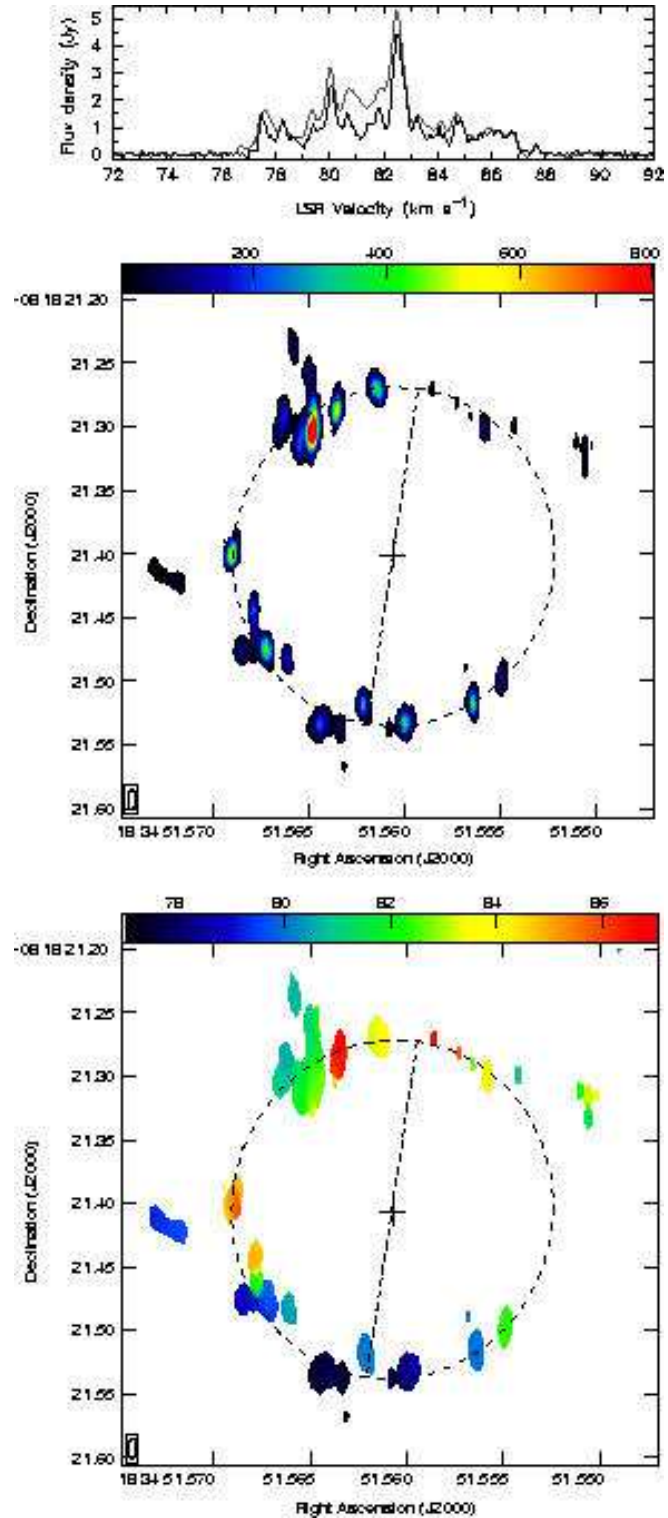
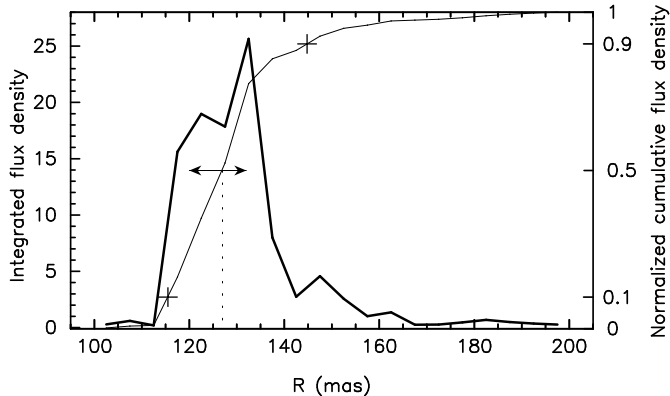


Fig. 1. The 6.7 GHz methanol maser from G23.657–0.127. *Top:* Spectrum of the integrated flux density from all the maser emission in the map (bold line) together with the Toruń total power spectrum (thin line) taken on 2005 February 2. *Middle:* Total intensity (zeroth moment) map. The colour scale varies linearly from 5 to $800 \text{ Jy beam}^{-1} \text{ m s}^{-1}$. The beam is indicated by the ellipse in the bottom left-hand corner of the image. The dashed ellipse shows the flux-weighted fit to the data while the dashed line indicates the orientation of the major axis. The cross indicates the inferred position of a central object. *Bottom:*

Table 1. The position of the centre of the G23.657–0.127 maser and the infrared counterparts.

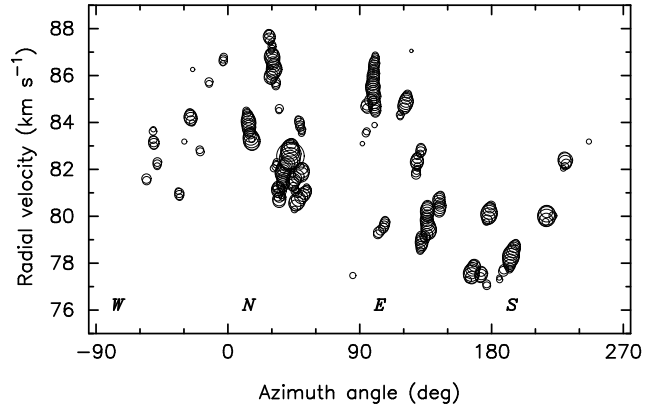
	RA(J2000)($^{\circ}$) ($18^{\text{h}}34^{\text{m}}$)	Dec.(J2000)($^{\circ}$) ($-08^{\circ}18'$)	Difference from radio position ($''$)	Reference
G23.657–0.127	51.5606 ± 0.0007	21.401 ± 0.012		this paper
2MASS183451.56–0818214	$51.56 \pm 0.0073(3)$	21.4 ± 0.11	0.087	2MASS (Cutri et al.2003)
G023.6566-00.1273	51.6 ± 0.02	22 ± 0.3	0.6	MSX6C (Egan et al.2003)
IRAS18321–0820	52.0 ± 0.96	20 ± 9.5	6.1	IRAS PSC (IPAC 1986)

**Fig. 2.** The integrated flux density per annulus of 5 mas (bold line) and the normalized cumulative flux density (thin line) versus radius. The radius of the maser ring at 50% of the total emission is marked by the dotted line. The width between a normalized cumulative flux density range of 25% to 75% (and 10% and 90%) is marked by the arrowed horizontal bar (and crosses).

$168 \text{ m s}^{-1} \text{ mas}^{-1}$. Fig. 3 shows the velocity of all components versus the azimuth angle between the maser spot and the major axis of the ellipse fitted in Fig. 1. Considerable velocity dispersion of $\sim 5.4 \text{ km s}^{-1}$ exists, but there is also a weak signature detectable with the dominant blue- and red-shifted emission originating from the southern and northern parts of the ring, respectively. It is also remarkably that the velocity gradients of the masers components are all dominantly radial.

4. Discussion

The most striking result from our VLBI observations is the detection of a nearly circular ring of maser emission. The symmetric distribution of maser components strongly suggests that they have a common origin and that there exists a central source. It is very remarkable and reassuring that the ring centre coincides with the infrared source 2MASS183451.56–0818214 within the position uncertainties. It also matches (2σ position uncertainty) with the object G023.6566-00.1273 in the MSX6C catalogue and lies well within the position error ellipse of IRAS18321–0820 (Table 1). Although one must remember that the infrared data were taken with a much coarser resolution, we derived the spectral energy distribution of the object, which is typical for embedded protostar(s) or recently formed high-mass star(s) (Fig. 4). A model of two black-body components (Walsh et al. 1999) reproduces the data satisfactory; the cold dust tem-

**Fig. 3.** Velocity of the maser spots in the ring versus azimuth angle measured from the major axis (north to east). The sizes of circles are proportional to the logarithm of the flux densities.

perature is 80 K and the hot dust temperature is 540 K. We note that this is a very crude estimate, as the 60 and 100 μm flux densities are poorly determined and millimeter wavelength emission was not yet measured. No radio continuum emission was found above a detection limit of $\sim 3 \text{ mJy}$ at 5 GHz (Giveon et al. 2005). Searches for other masers species were negative: neither H_2O masers at 22 GHz, nor any of the four OH masers at 1.6 GHz were found (Szymczak & Gérard 2004; Szymczak et al.2005). Only weak absorption features near 80 km s^{-1} appeared at 1665 and 1667 MHz (Szymczak & Gérard 2004).

Assuming that the central velocity of the methanol maser profile (82.4 km s^{-1}) is the systemic velocity and using the equation for the Galactic rotation curve given by Brand & Blitz (1993), we derived the near and far kinematic distances of G23.657–0.127 as 5.1 and 10.5 kpc, respectively. Applying the formula by Walsh et al. (1997; their equation 3) we estimated the bolometric luminosities from the mid- and far-infrared emission as: $\leq 3.2 \times 10^4 L_{\odot}$ and $\leq 1.2 \times 10^5 L_{\odot}$ for the near and far kinematic distances, respectively. If these luminosities are provided by single stars then these would correspond to B0 and O7 ZAMS stars (Panagia 1973). The luminosities are, however, most likely due to a cluster of stars, unresolved in the infrared (Walsh et al. 1997, 2001). For the near and far kinematic distances the average radius of the maser ring as determined in Sect. 3 is 650 AU and 1330 AU and its width is 60 AU and 130 AU, respectively.

In principle there are several three-dimensional structures that project onto a ring structure like we have observed. The fact that the maser components at velocities close to the central velocity resolve out into multiple directions can be interpreted as a circumstellar shell or a spherical bubble. However, a disc

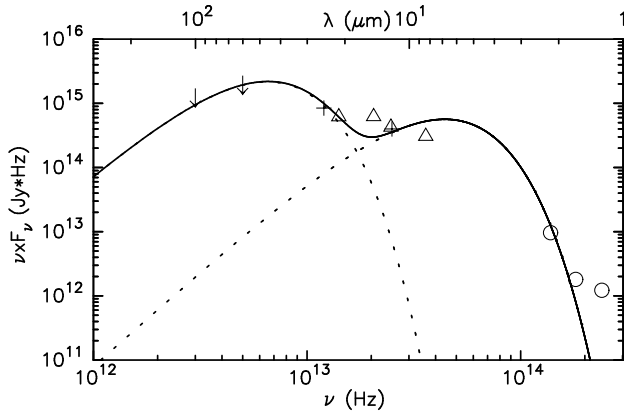


Fig. 4. Spectral energy distribution of G23.657–0.127. Data for counterparts (Table 1) in 2MASS (circles), MSX6C (triangles) and IRAS (crosses) are shown. The upper limits for IRAS are marked by arrows. A model of two black-body components (Walsh et al. 1999) is represented by the curved lines.

geometry seen face-on results in a similar structure. We discuss these options below.

A steep increase of the maser intensity at the inner edge of the ring and a smooth decrease at its outer edge suggest that the maser arises in a narrow circular layer of the excited material. One can imagine that the masers outline an expanding bubble and we observe a ring from the material in plane of the sky through tangential amplification. The bubble may be the shock front originating from the central star and propagating into the circumstellar gas. Assuming an expansion velocity of 5.4 km s^{-1} its dynamical age is $\sim 550 \text{ yr}$ or $\sim 1130 \text{ yr}$ for the near and far kinematic distances, respectively. A spherical bubble was recently also detected in Cep A by H_2O maser emission (Torrelles et al. 2003) and may occur as a short lived stage in the earliest stages of stellar evolution. The lack of detectable radio continuum at 5 GHz does not preclude the interpretation as a spherical shock from a young stellar object. It is quite possible that the ionization front around the central star(s) of G23.657–0.127 is too weak to be visible at 5 GHz or so dense that it becomes detectable only at higher frequencies (Carral et al. 1996). Alternatively, the result of shock wave may be limited to dense knots of compressed and accelerated gas without ionizing it (Phillips et al. 1998). The radial shock wave model offers a natural explanation of the observed filaments and arcs with internal velocity gradients.

The observed weakly elliptical structure (0.38 eccentricity) can be interpreted as a disc inclined at an angle of 68° . However, for a geometry so close to face-on the inclination and the orientation of the major axis are poorly constrained. One expects a weak velocity signature with the extreme velocities originating from where the ellipse intersects with the major axis. Such a velocity signature between the south and the north may be detected (Sect. 3), but the large uncertainty does not allow a convincing fit of a rotating disk to the data (Fig. 3). A complication of this model is that the methanol masers would need to be built up nearly perpendicular to the disc plane.

Previous claims of methanol discs all have derived edge-on geometries. This can be understood as a selection effect,

because the strongest masers may result from radial amplification. The current observations focused on sources with relatively low peak fluxes. We have been able to image many weak features because of the increased number of EVN antennas with 5 cm receivers. With the currently available data it is not possible to distinguish between the spherical bubble and the rotating disc models. Further observational verifications of these possibilities include high resolution studies of radio continuum, tracers of shock fronts as well as multi-epoch studies of methanol masers.

Acknowledgements. We thank to Bob Campbell at JIVE for his detailed support in many stages of this experiment and to an anonymous referee for useful comments. This work has benefited from research funding from the EC 6th Framework Programme and supported by the MNII grant 1P03D02729.

References

- Brand, J., & Blitz, L. 1993, *A&A*, 275, 67
- Carral, P., Kurtz, S.E., Rodriguez, L.F., de Pree, C., & Hofner, P. 1996, *ApJ*, 486, L103
- Cutri, R.M., Skrutskie, M.F., Van Dyk, S., et al. 2003, 2MASS All-Sky Catalog of Point Sources, <ftp://cdsarc.u-strasbg.fr/pub/cats/II/246>
- Dodson, R., Ojha, R., & Ellingsen, S.P. 2004, *MNRAS*, 351, 779
- Egan, M.P., Price S.D., Kraemer, K.E., et al. 2003, MSX6C Infrared Point Source Catalog, <ftp://cdsarc.u-strasbg.fr/pub/cats/V/114>
- Elitzur, M. 1992, *Astronomical Masers*, Kluwer, Dordrecht
- Giveon, U., Becker, R.H., Helfand, D.J., & White, R.L. 2005, *AJ*, 129, 348
- Joint IRAS Science W.G. 1986, IRAS Catalog of Point Sources, Version 2.0, <ftp://cdsarc.u-strasbg.fr/pub/cats/II/125>
- Menten, K.M. 1991, *ApJ*, 380, L75
- Minier, V., Booth, R.S., & Conway, J.E. 2000, *A&A*, 362, 1093
- Norris, R.P., Byleveld, S.E., Diamond, P.J., et al. 1998, *ApJ*, 508, 275
- Panagia, N. 1973, *AJ*, 78, 929
- Phillips, C.J., Norris, R.P., Ellingsen, S. P., & McCulloch, P. M. 1998, *MNRAS*, 300, 1131
- Szymczak, M., Kus, A.J., Hrynek, G., Kepa, A., & Pazderski, E. 2002, *A&A*, 392, 277
- Szymczak, M., & Gérard, E. 2004, *A&A*, 423, 209
- Szymczak, M., Pillai, T., & Menten, K.M. 2005, *A&A*, 434, 613
- Torrelles, J.M., Patel, N.A., Anglada, G., et al. 2003, *ApJ*, 598, L115
- Walsh, A.J., Bertoldi, F., Burton, M.G., & Nikola, T. 2001, *MNRAS*, 326, 36
- Walsh, A.J., Burton, M.G., Hyland, A.R., & Robinson, G. 1998, *MNRAS*, 301, 640
- 1999, *MNRAS*, 309, 905
- Walsh, A.J., Hyland, A.R., Robinson, G., & Burton, M.G. 1997, *MNRAS*, 291, 261